

COMPARATIVE ANALYSIS OF VORTEX METHOD SIMULATIONS OF THE FLOW AROUND A CIRCULAR CYLINDER USING A SOURCE PANEL METHOD AND THE CIRCLE THEOREM

Vanessa Gonçalves Guedes

Materials and Mechanics Area – CEPTEL
P.O. Box 68007
21944-970 Rio de Janeiro, RJ – Brazil
vanessag@cepel.br

Gustavo César Rachid Bodstein

Department of Mechanical Engineering – EE/COPPE/UFRJ
P.O. Box 68503
21945-970 Rio de Janeiro, RJ – Brazil
gustavo@serv.com.ufrj.br

Miguel Hiroo Hirata

Department of Mechanics, Mechanical Engineering Institute, EFEI
P.O. Box 50
37500-000 Itajubá, MG – Brazil
hirata@iem.efei.br

Abstract. External incompressible flows at high Reynolds numbers around bluff bodies are characterized by flow separation and the development of a Von Karman-type periodic wake. Many attempts to numerically simulate most of the flow details have been reported in the literature, and a variety of both mesh-based and mesh-free methods have been used. In this paper we use a mesh-free two-dimensional discrete vortex method to calculate the flow around a circular cylinder. The dynamics of the body wake is computed using the convection-diffusion splitting algorithm, where the diffusion process is simulated using the random walk method, and the convection process is carried out with a Lagrangian second-order time-marching scheme. Lamb vortices are generated along the cylinder surface, whose strengths are determined to ensure that the no-slip condition is satisfied and that circulation is conserved. Two methodologies are used to impose the impermeability condition: a source panel method, so that mass conservation is explicitly enforced, and the circle theorem. Results for the aerodynamic forces and pressure distribution obtained with the two methodologies are compared to each other and to other results available in the literature.

Keywords. Bluff Bodies, Unsteady Wake, Circle Theorem, Panel Method, Vortex Method.

1. Introduction

The Vortex Method has been extensively used over the last decades to study flows with regions of concentrated vorticity, such as separated flows around bluff bodies. Alternatively to the classical mesh-based (Eulerian) methods, all the different versions of the vortex method have been developed within either a mesh-free (Lagrangian) framework, or a hybrid (Eulerian-Lagrangian) framework. In the first case, purely Lagrangian techniques are adopted for the transport of vorticity, and no mesh is required (Kamemoto, 1994); in the second case, part of the calculation is carried out on a mesh, and part is performed according to a Lagrangian description (Smith and Stansby, 1988). Either framework presents advantages and disadvantages over the other, and the choice of one over the other depends on many factors, mainly the Reynolds number and the flow geometry. In the particular case of two-dimensional, unsteady, incompressible and high Reynolds number flows around bluff bodies, mesh-free (Lagrangian) vortex methods provide a suitable framework, the main reasons being: the absence of a mesh avoids stability problems of explicit schemes (or cumbersome implementation of implicit schemes) and mesh refinement problems in regions of high rates of strain; all the calculation is restricted to the rotational flow regions, and no explicit choice of the outer boundaries is needed a priori; no boundary condition is required at the downstream end of the flow domain. However, in mesh-free vortex methods the number of operations at each time step, which is governed by the convective step, is proportional to the square of the number of vortices present in the flow during the time step. This may lead to very large CPU times if a long-time solution is sought.

In this paper we compare two versions of a vortex method implementation to simulate the two-dimensional, incompressible, unsteady flow around a circular cylinder at a high Reynolds number: one based on the circle theorem, and the other based on the panel method. In the first algorithm, vortices with a Lamb core are generated along the cylinder surface. The application of the circle theorem imposes exactly the impermeability condition on the cylinder surface. A linear system of algebraic equations for the unknown vortex strengths is formed in order to explicitly ensure that the no-slip condition is satisfied and that circulation is conserved; this system is solved using the Singular Value Decomposition Method. The dynamics of the vorticity in the body wake is computed using the convection-diffusion splitting algorithm, where convection is carried out with a Lagrangian second-order Adams-Bashforth time-marching scheme and diffusion is simulated using the random walk method. In the second algorithm, the impermeability condition on the cylinder surface is imposed using the panel method with a constant strength source distribution on each

panel. A linear system of algebraic equations for the unknown vortex and source strengths is formed in order to explicitly ensure that the no-slip and the no-penetration conditions are satisfied and that circulation and mass are conserved; this system is also solved using the Singular Value Decomposition Method.

In the Circle Theorem Algorithm (CTA), the (virtual) image vortices which are present inside the circular cylinder resulting from the application of the circle theorem doubles the number of vortices in the flow. On one hand, this fact slows down the algorithm. On the other hand, the circle theorem guaranties that the impermeability condition is satisfied exactly along the entire cylinder surface (Mustto et al., 1998). With this implementation, the only way a different body geometry other than circular can be implemented is through a conformal mapping. Carreiro and Bodstein (2002) use this methodology to carry out vortex-method simulations for high Reynolds-number flows around elliptic cylinders.

In the Panel Method Algorithm (PMA), the potential flow due to the presence of the body is calculated using the panel method with constant strength source distribution. The panel distribution forms a closed polygon with a shape that approximates, as nearly as possible, the actual shape of the bluff body, in our case, the circular cylinder. The impermeability and the no-slip boundary conditions are imposed in the control points of the panels. This implementation leads to smaller CPU times and a large variety of body shapes can be analyzed, but the impermeability condition is satisfied only at the control points of the panels (Moran, 1984), differently from the CTA.

Our objective is to compare the results obtained with both algorithms to each other and to other results available in the literature. The basic equations that govern the problem under investigation are presented in the next section, followed by the numerical methods and the algorithms of both implementations, the CTA and the PMA. Results are then presented and discussed. The last section summarizes the conclusions.

2. MATHEMATICAL FORMULATION

2.1. The Flow Around a Circular Cylinder

We begin our analysis considering the flow around a circular cylinder of radius a , immersed in an unbounded region with a uniform flow and freestream speed U (Fig. 1). We assume the flow to be incompressible and two-dimensional, and the fluid to be newtonian with constant kinematic viscosity ν . The unsteady flow that develops originates from the separation that occurs on the cylinder surface, which generates an oscillatory wake downstream of the body. This flow is governed by the continuity and the Navier-Stokes equations, which can be written in the form

$$\nabla \cdot \mathbf{u} = 0, \quad (1)$$

$$\frac{\partial \mathbf{u}}{\partial t} + \mathbf{u} \cdot \nabla \mathbf{u} = -\nabla p + \frac{1}{\text{Re}} \nabla^2 \mathbf{u}. \quad (2)$$

In the equations above \mathbf{u} is the velocity vector field, p is the pressure, and $\text{Re} \equiv 2Ua/\nu$ is the Reynolds number based on the cylinder diameter $2a$. All the quantities in the Eqs. (1), (2) and the equations below are non-dimensionalized by U and a .

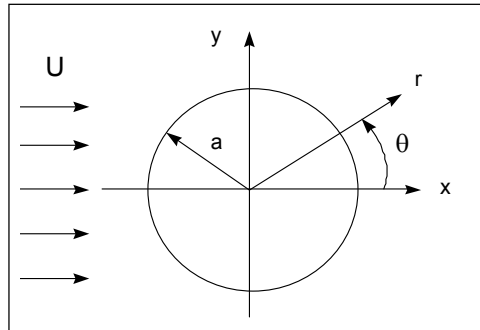


Figure 1. Flow around a circular cylinder.

For all the cases studied, the flow is started impulsively from rest. The impermeability and the no-slip boundary conditions on the surface of the cylinder can be expressed as

$$\mathbf{u}_n \equiv \mathbf{u} \cdot \mathbf{n} = 0, \quad \text{at } r = 1, \quad (3)$$

$$\mathbf{u}_t \equiv \mathbf{u} \cdot \mathbf{t} = 0, \quad \text{at } r = 1, \quad (4)$$

where \mathbf{n} and \mathbf{t} are unit vectors normal and tangential to the cylinder surface, respectively. At infinity we require that

$$|\mathbf{u}| \rightarrow 1, \text{ at infinity.} \quad (5)$$

The dynamics of the fluid motion, governed by the boundary-value problem (1)-(5), can be studied in a more convenient way if we take the curl of Eq. (2) to obtain the vorticity equation. For a 2-D flow this equation is scalar, and it can be written as

$$\frac{\partial \omega}{\partial t} + \mathbf{u} \cdot \nabla \omega = \frac{1}{\text{Re}} \nabla^2 \omega, \quad (6)$$

where ω is the only non-zero component of the vorticity vector (in a direction normal to the plane of the flow).

In our model, a cloud of N_v discrete point vortices, each of constant strength Γ_k , represents the flow vorticity. In CTA, we use the circle theorem (Milne-Thompson, 1955) to combine this point-vortex representation with a uniform flow and a dipole to construct a flow field such that Eqs. (1), (3) and (5) are automatically satisfied. Thus, a suitable mathematical expression for the velocity field in the complex z -plane, where $z = x + iy$, is given by

$$\mathbf{u} - i\mathbf{v} = \left(1 - \frac{1}{z^2}\right) - \frac{i}{2\pi} \sum_{k=1}^{N_v} \frac{\Gamma_k}{z - z_k(t)} + \frac{i}{2\pi} \sum_{k=1}^{N_v} \frac{\Gamma_k}{z - z_{k\text{im}}(t)}. \quad (7)$$

In Eq. (7) the first two terms on the right-hand side represent a uniform flow and a dipole, which account for the potential flow around a circular cylinder. The third term corresponds to the cloud of point vortices that model the vorticity in the boundary layer and wake, whereas the fourth term corresponds to the image vortices, which appear from the circle theorem to satisfy the impermeability condition, Eq. (3). The quantities in Eq. (7) are defined as follows: u and v are the components of \mathbf{u} in the x and y directions, respectively; z_k is the position of the k -th-point vortex with strength Γ_k , and $z_{k\text{im}} \equiv 1/z_k^*$ is the position of its image at the inverse point, where the “*” denotes complex conjugate; and N_v is the total number of vortices present in the flow (not considering their images). Note that the images at the origin, prescribed by the circle theorem, are neglected, since their presence affects the boundary condition at infinity (Sarpkaya, 1989).

In PMA, we use the source panel method (Anderson Jr., 1991) to superimpose the flows comprised of the vortex cloud, the uniform flow and the flow due to a source distribution on the N panels, each of constant strength per unit panel length λ_j , to construct a flow field that satisfies Eqs. (1), (3) and (5) automatically. Thus, the u and v velocities components of the total flow can be written in terms of the vortex and source strengths and the panel geometry according to the following equations

$$u(x, y) = \sum_{j=1}^N \frac{\lambda_j}{2\pi} \left(\frac{C_u}{2} \ln \left(\frac{\text{Sp}_j^2 + 2A\text{Sp}_j + B}{B} \right) + \frac{D_u - AC_u}{E} \left(\tan^{-1} \frac{\text{Sp}_j + A}{E} - \tan^{-1} \frac{A}{E} \right) \right) - \frac{1}{2\pi} \sum_{j=1}^{N_v} \Gamma_j \frac{(y - y_j)}{(x - x_j)^2 + (y - y_j)^2} \quad (8a)$$

$$v(x, y) = \sum_{j=1}^N \frac{\lambda_j}{2\pi} \left(\frac{C_v}{2} \ln \left(\frac{\text{Sp}_j^2 + 2A\text{Sp}_j + B}{B} \right) + \frac{D_v - AC_v}{E} \left(\tan^{-1} \frac{\text{Sp}_j + A}{E} - \tan^{-1} \frac{A}{E} \right) \right) + \frac{1}{2\pi} \sum_{j=1}^{N_v} \Gamma_j \frac{(x - x_j)}{(x - x_j)^2 + (y - y_j)^2}, \quad (8b)$$

where the constants above can be expressed in terms of the geometrical panel parameters, shown in Fig.2, as

$$A = -(x - Xp_j) \cos \varphi_j - (y - Yp_j) \sin \varphi_j, \quad (9a)$$

$$B = (x - Xp_j)^2 + (y - Yp_j)^2, \quad (9b)$$

$$C_u = -\cos(\varphi_j), \quad (9c)$$

$$D_u = x - Xp_j, \quad (9d)$$

$$\text{Sp}_j = \sqrt{(Xp_{j+1} - Xp_j)^2 + (Yp_{j+1} - Yp_j)^2}, \quad (9e)$$

$$E = \sqrt{B - A^2} = (x - Xp_j) \sin \varphi_j - (y - Yp_j) \cos \varphi_j, \quad (9f)$$

$$C_v = -\sin(\varphi_j), \quad (9g)$$

$$D_v = y - Yp_j. \quad (9h)$$

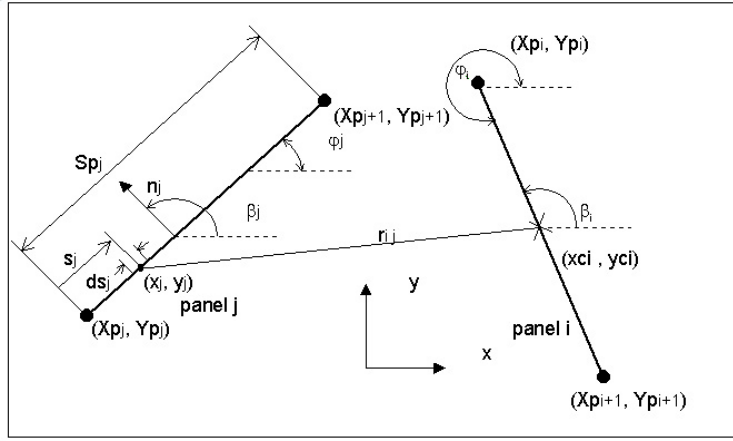


Figure 2. Geometry of the panels.

The aerodynamic force coefficients are calculated through integration of the pressure coefficient distribution around the circular cylinder, which takes the form

$$C_D = \int_0^{2\pi a} C_p \sin \varphi(s) ds \quad \text{and} \quad C_L = \int_0^{2\pi a} C_p \cos \varphi(s) ds \quad (10a, 10b)$$

where C_D and C_L are the drag and lift coefficients, respectively. In order to calculate the pressure coefficient, we develop a new algorithm, based on the algorithm proposed by He and Su (1998), such that C_p at a panel control point m is calculated according to the following expression

$$C_p = 1 + 2 \left(\sum_{n=1}^m \left(\frac{\Gamma_n}{\Delta t} - \Delta u_n \overline{u_n} \right) - \sum_{n=1}^{n_{\max}} \left(\frac{\Gamma_n}{\Delta t} - \Delta u_n \overline{u_n} \right) \right), \quad (11)$$

where $\Delta u_n = (u_{(+)} - u_{(-)})$ (12)

and $\overline{u_n} = \left(\frac{u_{(+)} + u_{(-)}}{2} \right)$. (13)

The velocities $u_{(+)}$ and $u_{(-)}$ are calculated at the upper corners of a control volume bounded by panel n and enclosing a nascent vortex adjacent to the panel, as shown in Fig. 3.

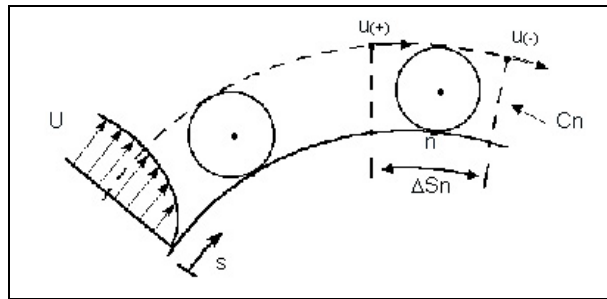


Figure 3. Tangential velocities at the upper corners of a control volume bounded by a panel and enclosing a nascent vortex adjacent to the panel.

3. THE VORTEX METHOD

3.1. The Algorithm

The two-dimensional, incompressible, unsteady flow around a circular cylinder formulated above is simulated using the Discrete Vortex Method developed by Musto et al. (1998), which is based on Eq. (6). This method uses an algorithm that splits the convective-diffusive operator (Chorin, 1973) in the form

$$\frac{D\omega}{Dt} \equiv \frac{\partial\omega}{\partial t} + \mathbf{u} \cdot \nabla\omega = 0 \quad (15)$$

$$\frac{\partial\omega}{\partial t} = \frac{1}{Re} \nabla^2 \omega . \quad (16)$$

In a real flow vorticity is generated on the body surface so as to satisfy the no-slip condition, Eq. (4), and is transported by convection and diffusion into the flow according to Eq. (6). Our discrete vortex method represents the vorticity by discrete vortices, whose transport by convection and diffusion is carried out in a sequence within the same time step. First, a lagrangian approach is used to simulate the convective process, governed by Eq. (15). The convective motion of each vortex is determined by integration of each vortex path equation, which can be written, using a second-order Adams-Bashforth scheme, as

$$\Delta x_c = \left[\frac{3}{2}u(t) - \frac{1}{2}u(t - \Delta t) \right] \Delta t \quad \text{and} \quad \Delta y_c = \left[\frac{3}{2}v(t) - \frac{1}{2}v(t - \Delta t) \right] \Delta t . \quad (17a, 17b)$$

In Eqs. (17a) and (17b), Δx_c and Δy_c are displacements of a vortex owing to convection, and u and v are components of the velocity at the point occupied by the vortex. Second, the process of viscous diffusion, governed by Eq. (16), is simulated using the Random Walk Method (Lewis, 1991), where the random displacements of each vortex in the x and y directions owing to diffusion, Δx_d and Δy_d , are calculated from

$$\Delta x_d = \Delta r \cos(\Delta\theta) \quad \text{and} \quad \Delta y_d = \Delta r \sin(\Delta\theta) , \quad (18a, 18b)$$

$$\Delta r = \left[8Re^{-1} \Delta t \ln(1/P) \right]^{1/2} , \quad \text{and} \quad \Delta\theta = 2\pi Q . \quad (19a, 19b)$$

In the Eqs. (19a) and (19b), P and Q are random numbers between 0 and 1 drawn from a uniform probability density distribution.

In order to remove the singularity of the point vortices we use Lamb vortices for $r \leq \sigma_o$, where σ_o is the radius of the vortex core. During a time step Δt , the core grows from zero to σ_o , where

$$\sigma_o = 6.34025 \sqrt{\frac{\Delta t}{Re}} . \quad (20)$$

This value is kept constant for the entire simulation. In terms of σ_o , the dimensionless velocity induced by the k -th vortex in the circumferential direction, $u_{\theta k}$, is

$$u_{\theta k} = \Gamma_k / 2\pi r \{1 - \exp[-C(r^2/\sigma_o^2)]\} . \quad (21)$$

In this particular equation r is the radial distance between the vortex center and the point in the flow field where the induced velocity is calculated, and $C = 5.02572$ is a constant. The distance ε off the cylinder surface where the new vortices are generated per time step (Fig. 3) is set equal to σ_o for all the cases studied.

The time step Δt is calculated from an estimative of the convective length and velocity scales of the flow. For a length scale Δs between vortices generated at the surface ($\sim 2\pi/N$) and a velocity scale of order one, we can write

$$\Delta t = \frac{2\pi k}{N} . \quad (22)$$

In Eq. (22), $0 < k \leq 1$, and N is the number of vortices generated per time step.

3.2. The Numerical Implementation

The numerical method described above is implemented essentially in five steps: (i) generation of new vortices; (ii) calculation of the forces on the body; (iii) convection of the vortices; (iv) diffusion of the vortices; (v) reflection of some vortices; (vi) stepping in time.

In the CTA, the process of vorticity generation is carried out so as to satisfy the no-slip condition, Eq. (4). According to the discussion above the circle theorem guarantees that the impermeability condition is satisfied exactly on the cylinder surface. At each time step, N new vortices are created at a small distance ε off the body surface, at a

radial distance $(1 + \varepsilon)$ to be more precise, with a uniform angular distribution. The strengths of these new vortices are determined by imposing the no-slip condition at N points on the cylinder surface, right underneath the newly created vortices (Fig. 4a). In order to implement the entire procedure, the velocities induced by all the vortices in the wake (and their images) are computed at the N points where Eq. (4) must be satisfied. This contribution is added to the velocities induced by the new vortices (and their images) and equated to zero. Thus, N equations can be written out for the N unknowns (the strengths of the new vortices). The last equation is a statement of conservation of circulation, where the sum of all vortices, with known and unknown strengths (and their images) must equal zero. This procedure yields an algebraic system of $N+1$ equations and N unknowns, that is,

$$\sum_{k=1}^N A_{jk} \Gamma_k(t) = b_j(t), \quad 1 \leq j \leq N, \quad (23)$$

$$\sum_{k=1}^N \Gamma_k(t) = b_{N+1}(t). \quad (24)$$

The elements of the $(N+1) \times N$ matrix, A_{jk} , depend only on the position of the vortices just created and on the points on the cylinder surface where the no-slip condition is imposed. It is, therefore, calculated only once for the entire simulation. The vector b_j , which is recalculated every time step, includes the contribution of all the terms in Eq. (7). The vortices that penetrate the body (due to the convective and/or diffusive motion) are reflected. In this implementation, the $(N+1) \times N$ system defined by Eqs. (23) and (24) is written in the form $\mathbf{Ax} = \mathbf{b}$ and the Singular Value Decomposition Method (Press et al., 1989) is used to solve it.

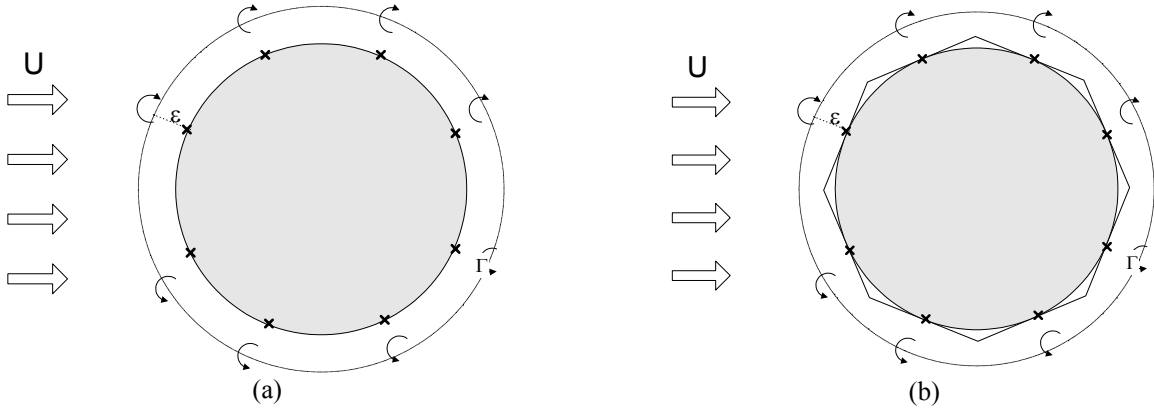


Figure 4. (a) Vortex generation scheme in the CTA. (b) Vortex generation scheme in the PMA.

In PMA, the process of vorticity generation is carried out so as to satisfy the impermeability and the no-slip conditions, Eqs. (3) and (4), simultaneously. At each time step, N new nascent vortices are created at a small distance ε off the body surface, just above of the panel control points (Fig. 4b), and N new sources are created on the N panel control points. The strengths of these new vortices and panel sources are determined by imposing the no-slip and the impermeability conditions simultaneously at the N panel control points on the cylinder surface. In order to implement the entire procedure, the velocities induced by all the vortices in the wake are computed at the N control points where Eqs. (3) and (4) must be satisfied. This contribution is added to the velocities induced by the new vortices and panel sources and equated to zero. Hence, $2N$ equations can be written out for the $2N$ unknowns (N new vortex strengths and N new source strengths). We also add two extra equations, which are statements of conservation of circulation (the sum of all vortices with known and unknown strengths must equal zero) and mass (the sum of all new source strengths must equal zero). This procedure yields an algebraic system of $2N+2$ equations and $2N$ unknowns, that is

$$\sum_{k=1}^N (A_{jk} \Gamma_k(t) + B_{jk} \lambda_k(t)) = b_j(t), \quad 1 \leq j \leq N, \quad (25)$$

$$\sum_{k=1}^N (C_{jk} \Gamma_k(t) + D_{jk} \lambda_k(t)) = b_j(t), \quad 1 \leq j \leq N, \quad (26)$$

$$\sum_{k=1}^N \Gamma_k(t) = b_{2N+1}(t), \quad (27)$$

$$\sum_{k=1}^N \lambda_k(t) = b_{2N+2}(t), \quad (28)$$

Guedes et al. (2002) solves the system above (Eqs. 25 to 28) by relaxing the no-slip and the impermeability conditions written out for the control point at $j = N/2$ (central panel on the cylinder backward face). Hence, removing two equations renders the new $(2N) \times (2N)$ system determined. Although very commonly used in linear systems of algebraic equations obtained from panel methods (Anderson, 1991), this procedure is hard to justify if all equations come from the same source (Strang, 1988). In addition, the usually small error component produced by this scheme adds up as the simulation evolves in time, since one new vortex that does not satisfy both the no-slip and the impermeability conditions is generated every time step. In our new scheme, on the other hand, we remove only the no-slip condition on panel $j = N/2$ to form a $(2N+1) \times (2N)$ system and we use the Singular Value Decomposition Method (Press et al., 1989) to solve it. If the linear system is written in the form $\mathbf{Ax} = \mathbf{b}$, this method consists of searching for a least squares solution that satisfies the “normal equations” (Strang, 1988), i.e.,

$$\mathbf{A}^T \mathbf{Ax} = \mathbf{A}^T \mathbf{b} . \quad (29)$$

Since the columns of the matrix \mathbf{A} are linearly independent, the matrix $\mathbf{A}^T \mathbf{A}$ is an invertible square matrix and $\bar{\mathbf{x}} = (\mathbf{A}^T \mathbf{A})^{-1} \mathbf{A}^T \mathbf{b}$, where the solution vector $\bar{\mathbf{x}}$ is the vector of the unknown Γ 's and λ 's that minimizes the error E of the solution in the least squares sense (Strang, 1988), where $E \equiv \|\mathbf{A}\bar{\mathbf{x}} - \mathbf{b}\|$. The linear system of algebraic equations $\mathbf{Ax} = \mathbf{b}$, written in matrix form, is given by

$$\begin{bmatrix} A_{jk} & B_{jk} \\ C_{jk} & D_{jk} \\ 1 & 0 \\ 0 & 1 \end{bmatrix}_{2N+1, 2N} \begin{bmatrix} \Gamma_k(t) \\ \lambda_k(t) \end{bmatrix}_{2N} = \begin{bmatrix} b_j(t) \end{bmatrix}_{2N+1} . \quad (30)$$

In the $(2N+1) \times (2N)$ matrix \mathbf{A} , the $N \times N$ submatrix A_{jk} represents the coefficient matrix of the normal velocities induced by all the vortices, the $N \times N$ submatrix B_{jk} represents the coefficient matrix of the normal velocities induced by the source panels, the $N \times N$ submatrix C_{jk} represents the coefficient matrix of the tangential velocities induced by the vortices, and the $N \times N$ submatrix D_{jk} represents the coefficient matrix of the tangential velocities induced by the source panels. The third and fourth rows, given by Eqs. (27) and (28), represent the conservation of vorticity and mass, respectively. The elements of the $(2N+1) \times (2N)$ matrix \mathbf{A} depend on the position of the nascent vortices and panel control points on the cylinder surface where the no-slip and impermeability conditions are imposed, which do not change in time. Therefore, this matrix is calculated only once for the entire simulation. The vector $b_j(t)$ includes the contribution of all the terms in Eqs. (8) and (9) and, therefore, it is recalculated every time step.

4. RESULTS AND ANALYSIS

We now present the results for the full simulation of the high Reynolds number, two-dimensional, incompressible, unsteady flow around a circular cylinder using CTA and PMA. Aiming at demonstrating the performance of both algorithms for long-time simulations, two long-time runs were performed with 64 vortices generated per time step and $t = 50.00$, more than six times the longest simulation carried out by Koumoutsakos and Leonard (1995) for $Re = 9500$, their maximum value. Here, only the case $Re = 10^5$ was chosen, since this value of the Reynolds number is one order of magnitude higher than the maximum value chosen by Koumoutsakos and Leonard. Furthermore, the experimental drag coefficient and Strouhal number for $Re = 10^5$ are in a range where they are approximately constant with respect to the Reynolds number, and still within the subcritical regime. The numerical parameters used in the computations are: $\Delta t = 0.05$, $k = 0.50$, and $\varepsilon = \sigma_0 = 0.0045$. Both runs ended with 64000 vortices each.

The flow around a circular cylinder presents several interesting characteristics, which can be described starting with the occurrence of the separation phenomenon. Due to the blunt geometry of the cylinder, the pressure gradient becomes adverse on the frontal part of the cylinder surface, triggering separation and a vortex shedding mechanism. For the value of the Reynolds number investigated in this work, experiments show the formation of the so-called Von Karman vortex street, which is comprised of large vortices generated and shed alternately from the upper and lower surfaces of the cylinder. The vortices in the wake are connected in pairs by a vortex sheet. Owing to the periodic characteristics of the wake, the lift force on the cylinder oscillates in time around zero, with a frequency determined by the Strouhal number. The periodic behavior of the wake is also reflected on the drag force, which presents a time evolution that oscillates around a non-zero mean value. However, its non-dimensional frequency is twice the Strouhal number, since the drag force reaches its maximum value twice for each cycle of the lift force. For these reasons, the experimental values available in the literature represent time averages for the lift and drag coefficients.

Figure 5 and Fig. 7 illustrates the positions of the vortices present in the flow simulation at $t = 50.00$, for CTA and PMA, respectively. Both wakes clearly show the occurrence of separation on the cylinder surface, followed by the generation and growth of the separated vortices on the back of the cylinder, which precedes their shedding into the wake. It can also be seen the formation of pairs of the large eddies that comprise the Von Karman vortex street,

connected to each other by thin vortex sheets. The cores of these large vortices grow as they move downstream of the cylinder due to the diffusive effect of the flow. Note that the farthest vortices in the wake are generated at the initial moments of the simulation, and they are, therefore, subject to a numerical transient effect.

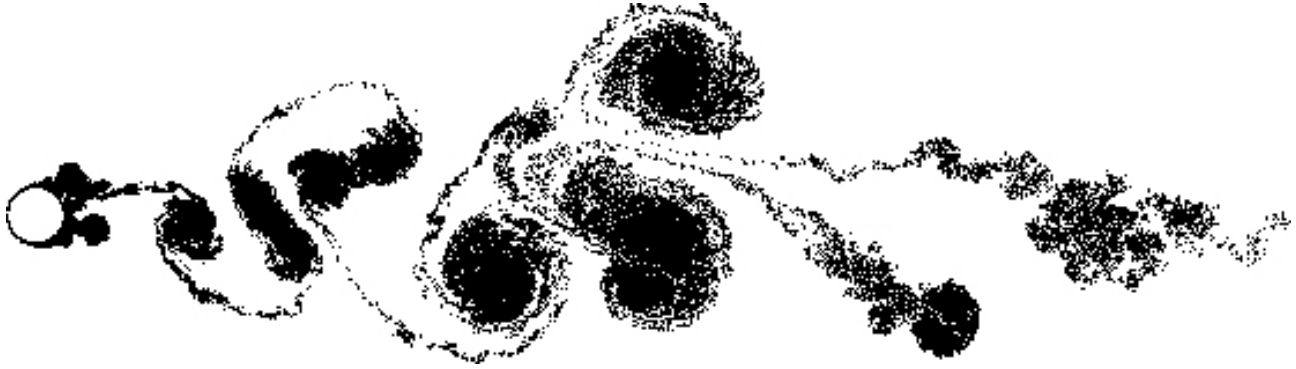


Figure 5. Positions of the wake vortices for $Re = 10^5$, at $t = 50.0$; $N = 64$, $\Delta t = 0.05$ and $\varepsilon = \sigma_0 = 0.0045$ using CTA.

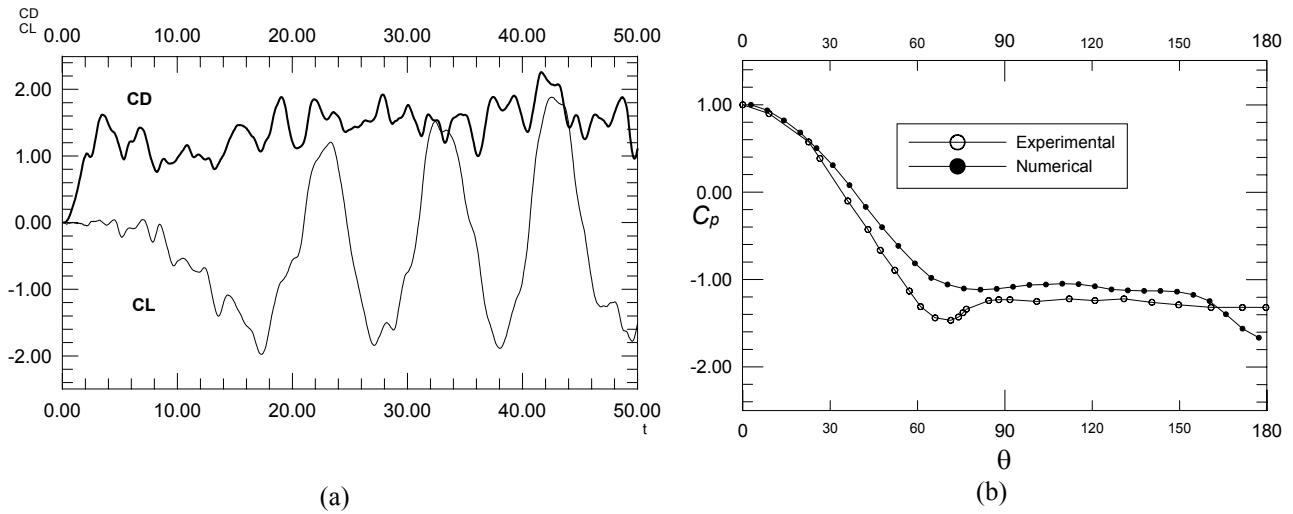


Figure 6. (a) Time variation of C_D and C_L for $Re = 10^5$, at $t = 50.0$; $N = 64$, $\Delta t = 0.05$ and $\varepsilon = \sigma_0 = 0.0045$ using CTA; (b) C_p distribution on the cylinder surface at $t = 50.0$, for $Re = 10^5$, $N = 64$, $\Delta t = 0.05$ and $\varepsilon = \sigma_0 = 0.0045$ using CTA.

The time histories of the lift and drag coefficients are revealed in Fig. 6 and in Fig. 8. As expected these coefficients reach a periodic steady state after an initial numerical transient (about 20 units of non-dimensional time), where they oscillate in time with approximately constant amplitude. The lift coefficient oscillates about zero with a non-dimensional frequency (Strouhal number, St) of 0.200, for CTA and 0.174 for PMA. These values are calculated using the C_L peaks at $t = 23.0$ and $t = 43.0$, for CTA, and using the C_L peaks at $t = 25.5$ and $t = 37.0$ for PMA. CTA presents a little higher value than the experimental one of Blevins' (1984), who measured 0.19, and PMA presents a little lower value than the experimental one of Blevins' (1984), with errors of 5.3% and 8.4%, respectively.

On the other hand, in CTA, the drag force oscillates about a mean value of 1.61 and, in PMA, the drag force oscillates about a mean value of 1.42 (integrated over the same cycle used to determine each St), with a non-dimensional frequency approximately equal to twice the Strouhal number. The experimental mean drag coefficient of Blevins' is 1.20, whereas the numerical value of Ogami and Ayano (1995) is 1.07. The comparison of our simulations with the experimental results of Blevins (1984) and the numerical results of Ogami and Ayano (1995) are shown in Table 1 for easy comparison. Ogami and Ayano's simulation was carried out using their viscous vortex method, called the Diffusion Velocity Method. As one can see, the agreement between our numerical methods and Ogami and Ayano's method is very good for the mean drag coefficient (Ogami and Ayano do not furnish results for the Strouhal number), and both results are close to the experimental value. However, for the value of the Reynolds number considered here, three-dimensional effects are always present in the experiments, whereas the simulations are purely two-dimensional. Therefore, the computations produce higher values for the drag coefficient, as obtained for our simulation. From this point of view, our simulations are more accurate than the one obtained by Ogami and Ayano (1995).



Figure 7. Positions of the wake vortices for $Re = 10^5$, at $t = 50.0$; $N = 64$, $\Delta t = 0.05$ and $\varepsilon = \sigma_0 = 0.0045$ using PMA.

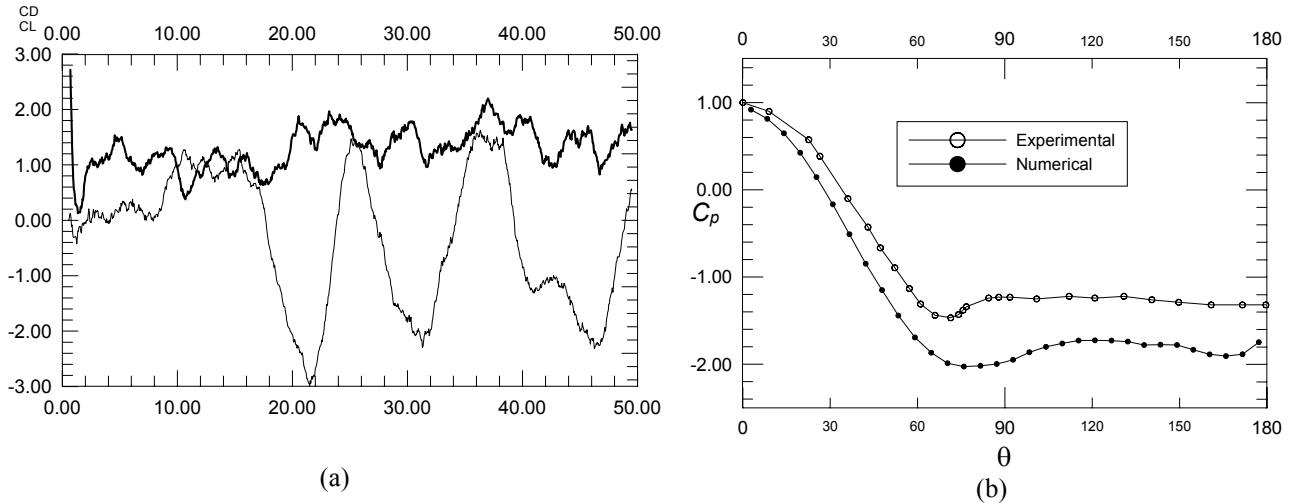


Figure 8. (a) Time variation of C_D and C_L for $Re = 10^5$, at $t = 50.0$; $N = 64$, $\Delta t = 0.05$ and $\varepsilon = \sigma_0 = 0.0045$ using PMA; (b) C_p distribution on the square cylinder surface at $t = 50.0$, for $Re = 10^5$, $N = 64$, $\Delta t = 0.05$ and $\varepsilon = \sigma_0 = 0.0045$ using PMA.

In Table 1 and the graphs presented in Fig. 6 and in Fig. 8, we can compare the results for the aerodynamic forces and pressure distribution of both implementations. Comparing the time histories of the lift and drag coefficients, we can notice that the results presented by CTA are more defined and smoother than the ones of PMA.

The Circle Theorem Algorithm presents better results than the Panel Method Algorithm because the impermeability boundary condition is satisfied over the entire circular cylinder surface and the no-slip boundary condition is satisfied only at the control points, whereas, in PMA, both impermeability and no-slip conditions are satisfied only at the panel control points. Both implementations used the Singular Value Decomposition Method, but in PMA, it was necessary to add two conservation equations (mass and vorticity conservation). Because the Singular Value Decomposition Method does not produce good results when the algebraic system has $2N+2$ equations and N unknowns, we relax the no-slip condition at the $N/2$ panel and work with $2N+1$ equations. This means that one vortex is generated without satisfying the no-slip boundary condition every time step.

On the other hand, CTA presents longer CPU times because of the presence of images inside the cylinder, showed in Eq. (7). As seen in Table 1, CTA presents a CPU time simulation about 4 times longer than the PMA CPU time. In addition, PMA allows other geometries to be easily simulated with good agreement with experimental results (Guedes et al, 2002 and Guedes et al, 2003), being necessary only to change the panel coordinates and other little adjustments in the reflection procedure of the vortices that enter the body during the simulation.

Table 1. Numerical Results for Circle Theorem Algorithm (CTA) and Panel Method Algorithm (PMA) and Experimental Results.

Algorithm	CPU time	Cd	St	Reference	Cd	St
Circle Theorem Algorithm (CTA)	72h.56min.	1.61	0.200	Blevins (1984): experimental	1.20	0.190
Panel Theorem Algorithm (PMA)	18h.33min.	1.42	0.174	Ogami e Ayano (1995): numerical	1.07	-

5. CONCLUSIONS

A comparative analysis to study the incompressible, two-dimensional, unsteady flow around a circular cylinder is performed to evaluate two versions of the discrete point vortex method: one that uses the circle theorem and another that uses a constant-strength source panel method.

In summary, CTA presents more accurate calculations of the force coefficients and Strouhal number than PMA because the impermeability boundary condition is satisfied over the entire circular cylinder surface and the no-slip boundary condition is satisfied only at the panel control points, whereas, in PMA, both the impermeability and the no-slip conditions are satisfied only at the panel control points. On the other hand, CTA presents longer CPU times because of the generation of image vortices inside the cylinder. In our simulations, CTA presents a CPU time about 4 times the PMA CPU time. PMA has also the advantage of allowing other geometries to be easily simulated with good agreement to experimental data.

6. ACKNOWLEDGEMENTS

The authors would like to acknowledge the Brazilian National Council for Scientific and Technological Development (CNPq), under grants AI 521260/94-9, AI 551364/02-5, 143041/97-5 and APQ 474904/01-6, and FAPEMIG, under grant no. TEC-1565/97, for their financial support during this project.

7. REFERENCES

- Anderson, J.D., 1991. "Fundamentals of Aerodynamics", 2nd. Edition, McGraw Hill.
- Bleviss, R.D., 1984, Applied Fluid Dynamics Handbook, Van Nostrand Reinhold Co.
- Chorin, A.J., 1973, Numerical Study of Slightly Viscous Flow, *Journal of Fluid Mechanics*, Vol. 57, pp. 785-796.
- Carreiro, F.R. and Bodstein, G.C.R., 2002, Numerical Simulation of the Unsteady Flow around Elliptic Cylinders Via the Joukowski Transformation, 9th Brazilian Congress of Thermal Engineering and Sciences - Encit 2002, Caxambu, M.G., pp. 1-10.
- He, F. and Su, T.C., 1998, A Numerical study of bluff body aerodynamics in high Reynolds number flows by viscous Vortex Element Method, *Journal of Wind Engineering and Industrial Aerodynamics*, Vols.77 e 78, pp.: 393-407.
- Guedes, V.G., Bodstein, G.C.R. and Hirata, M.H., 2002, Numerical Simulation of the Flow Around a Square Cylinder Using the Vortex Method, 9th Brazilian Congress of Thermal Engineering and Sciences - Encit 2002, Caxambu, M.G., pp. 1-9.
- Guedes, V.G., Bodstein, G.C.R. and Hirata, M.H., 2003, Numerical Simulation of the Flow around Rectangular Cylinders using the Vortex Method, *Proceedings of Third International Conference on Computational Heat and Mass Transfer*, May 26–30, 2003, Banff, Canada.
- Kamemoto, K., 1994, Development of Vortex Methods for Grid-Free Lagrangian Direct Numerical Simulation, *Proceedings of the 3th. JSME-KSME Fluids Engineering Conference*, July 25-27, Sendai, Japan.
- Koumoutsakos P. and Leonard, A., 1995, High-Resolution Simulations of the Flow Around an Impulsively Started Cylinder Using Vortex Methods, *Journal of Fluid Mechanics*, Vol. 296, pp. 1-38.
- Lewis, R.I., 1991, *Vortex Element Methods for Fluid Dynamic Analysis of Engineering Systems*, Cambridge University Press, Cambridge.
- Milne-Thomson, L. M., *Theoretical Hydrodynamics*, MacMillan & Co., 1955.
- Moran, J., 1984. "An Introduction to Theoretical and Computational Aerodynamics", John Wiley.
- Mustto, A. A., Hirata, M.H. and Bodstein, G.C.R., 1998, Discrete Vortex Method Simulation of the Flow Around a Circular Cylinder with and Without Rotation, *AIAA Paper 98-2409*, 16th. Applied Aerodynamics Conference, Albuquerque, N.M., June 15-18.
- Ogami, Y. and Ayano, Y., 1995, Flows Around a Circular Cylinder Simulated by the Viscous Vortex Method - The Diffusion Velocity Method, *Computational Fluid Dynamics Journal*, Vol. 4, No. 3, pp. 383-399.
- Press, W.H., Flannery, B.P., Teukolsky, S.A. and Vetterling, W.T., 1989, *Numerical Recipes -The Art of Scientific Computing*, Fortran version, Cambridge University Press.
- Sarpkaya, T., 1989, Computational Methods with Vortices - The 1988 Freeman Scholar Lecture, *Journal of Fluids Engineering*, Vol. 111, pp. 5-52.
- Smith, P.A. and Stansby, P.K., 1988, Impulsively Started Flow Around a Circular Cylinder by the Vortex Method, *Journal of Fluid Mechanics*, vol. 194, pp. 45-77.
- Strang, G., 1988, *Linear Algebra and Its Applications*, Harcourt Brace Jovanovich, 3rd. Edition.